

1-2018


Lateral diffusion and signaling of receptor for advanced glycation end-products (RAGE): a receptor involved in chronic inflammation

Aleem Syed
Iowa State University

Qiaochu Zhu
Iowa State University

Emily A. Smith
Iowa State University and Ames Laboratory, esmith1@iastate.edu

Follow this and additional works at: https://lib.dr.iastate.edu/chem_pubs

 Part of the [Analytical Chemistry Commons](#), [Biological Phenomena](#), [Cell Phenomena](#), and [Immunity Commons](#), [Biophysics Commons](#), and the [Cell Biology Commons](#)

The complete bibliographic information for this item can be found at https://lib.dr.iastate.edu/chem_pubs/1227. For information on how to cite this item, please visit <http://lib.dr.iastate.edu/howtocite.html>.

This Article is brought to you for free and open access by the Chemistry at Iowa State University Digital Repository. It has been accepted for inclusion in Chemistry Publications by an authorized administrator of Iowa State University Digital Repository. For more information, please contact digirep@iastate.edu.

Lateral diffusion and signaling of receptor for advanced glycation end-products (RAGE): a receptor involved in chronic inflammation

Abstract

Membrane diffusion is one of the key mechanisms in the cellular function of receptors. The signaling of receptors for advanced glycation end-products (RAGE) has been extensively studied in the context of several pathological conditions, however, very little is known about RAGE diffusion. To fill this gap, RAGE lateral diffusion is probed in native, cholesterol-depleted, and cytoskeleton-altered cellular conditions. In native GM07373 cellular conditions, RAGE has a 90% mobile fraction and an average diffusion coefficient of 0.3 $\mu\text{m}^2/\text{s}$. When depolymerization of the actin cytoskeleton is inhibited with the small molecule jasplakinolide (Jsp), the RAGE mobile fraction and diffusion coefficient decrease by 22 and 37%, respectively. In contrast, depolymerizing the filamentous actin cytoskeleton using the small molecule cytochalasin D (CD) does not alter the RAGE diffusion properties. There is a 70 and 50% decrease in phosphorylation of extracellular signal-regulated kinase (p-ERK) when the actin cytoskeleton is disrupted by CD or Jsp, respectively, in RAGE-expressing GM07373 cells. Disrupting the actin cytoskeleton in GM07373 cells that do not express detectable amounts of RAGE results in no change in p-ERK. Cholesterol depletion results in no statistically significant change in the diffusion properties of RAGE or p-ERK. This work presents a strong link between the actin cytoskeleton and RAGE diffusion and downstream signaling, and serves to further our understanding of the factors influencing RAGE lateral diffusion.

Keywords

Fluorescence recovery after photobleaching, Phosphorylation of ERK, Cell membrane biophysics, Actin cytoskeleton, Cholesterol depletion

Disciplines

Analytical Chemistry | Biological Phenomena, Cell Phenomena, and Immunity | Biophysics | Cell Biology

Comments

This is a post-peer-review, pre-copyedit version of an article published in *European Biophysics Journal*. The final authenticated version is available online at: <http://dx.doi.org/10.1007/s00249-017-1227-5>.
Posted with permission.

1 **Lateral Diffusion and Signaling of Receptor for Advanced Glycation End-products**
2 **(RAGE): A Receptor Involved in Chronic Inflammation**

3 **Aleem Syed¹, Qiaochu Zhu¹ and Emily A. Smith**

4 Department of Chemistry, Iowa State University, 1605 Gilman Hall, Ames, IA 50011

5 1 Both authors contributed equally

6 *esmith1@iastate.edu, (+1) 515-294-1424 (P), (+1) 515-294-0105 (F)

7

8 **Abstract**

9 Membrane diffusion is one of the key mechanisms in the cellular function of receptors. The
10 signaling of receptor for advanced glycation end-products (RAGE) has been extensively studied
11 in the context of several pathological conditions, however, very little is known about RAGE
12 diffusion. To fill this gap, RAGE lateral diffusion is probed in native, cholesterol depleted and
13 cytoskeleton altered cellular conditions. In native GM07373 cellular conditions, RAGE has a
14 90% mobile fraction and an average diffusion coefficient of $0.3 \mu\text{m}^2/\text{s}$. When depolymerization
15 of the actin cytoskeleton is inhibited with the small molecule Jasplakinolide (Jsp), the RAGE
16 mobile fraction and diffusion coefficient decrease by 22% and 37%, respectively. In contrast,
17 depolymerizing the filamentous actin cytoskeleton using the small molecule cytochalasin D (CD)
18 does not alter the RAGE diffusion properties. There is a 70% and 50% decrease in
19 phosphorylation of extracellular signal-regulated kinase (p-ERK) when the actin cytoskeleton is
20 disrupted by CD or Jsp in RAGE expressing GM07373 cells. Disrupting the actin cytoskeleton in
21 GM07373 cells that do not express detectable amounts of RAGE results in no change in p-ERK.
22 Cholesterol depletion results in no statistically significant change in the diffusion properties of
23 RAGE or p-ERK. This work presents a strong link between the actin cytoskeleton and RAGE
24 diffusion and downstream signaling, and serves to further our understanding of the factors
25 influencing RAGE lateral diffusion.

26 **Keywords** Fluorescence recovery after photobleaching, phosphorylation of ERK, cell membrane
27 biophysics, actin cytoskeleton, cholesterol depletion

28

29

30 **Introduction**

31 Lateral diffusion of membrane proteins is often interrelated with their cellular signaling and
32 functions in the cell membrane (Axelrod 1983; Ganguly *et al.* 2008; Ronchi *et al.* 2008). The
33 receptor for advanced glycation endproducts (RAGE) is a transmembrane protein that belongs to
34 the immunoglobulin (Ig) superfamily. Many RAGE ligands have been identified, including
35 advanced glycation endproducts (AGEs), S100 proteins, high mobility group box 1 (HMGB1),
36 and amyloid- β fibrils (Koch *et al.* 2010; Leclerc *et al.* 2009; Schmidt *et al.* 1992; Taguchi *et al.*
37 2000; Yan *et al.* 1996). RAGE and its signaling are associated with many disease states,
38 including some types of cancer, retinal disease, cardiovascular disease, Alzheimer's disease,
39 respiratory disorders, chronic inflammation and diabetic complications (Barile and Schmidt
40 2007; Basta 2008; Bierhaus and Nawroth 2009; Briot *et al.* 2009; Hofmann *et al.* 1999; Logsdon
41 *et al.* 2007; Yan *et al.* 2009). RAGE is reported to activate various signaling cascades, including
42 mitogen-activated protein kinases (MAPKs), Rac/Cdc42 and Janus kinases (JAK)/signal
43 transducers and activators of transcription (STATs) and NF- κ B (Ghavami *et al.* 2008; Hermani
44 *et al.* 2006; Huttunen *et al.* 1999; Lander *et al.* 1997; Wang *et al.* 2008; Yeh *et al.* 2001).
45 Through these signaling pathways, RAGE influences cell survival, motility and the inflammatory
46 response. Even though RAGE signaling has been studied extensively in different disease states,
47 very little is reported regarding RAGE diffusion in the cell membrane. The goal of the current
48 study is to investigate the lateral diffusion and cellular signaling of RAGE in the endothelial cell
49 membrane and to study the effects of cholesterol depletion and alterations to the actin
50 cytoskeleton on these properties.

51 Cholesterol and the actin cytoskeleton play an important role in the organization of the
52 cell membrane. Functional domains in the cell membrane, known as lipid rafts or lipid

53 nanodomains, contain about 3 to 5-fold excess cholesterol compared to neighboring regions of
54 bilayer (Ando *et al.* 2015; Lingwood and Simons 2010; Pike 2003; Simons and Gerl 2010).
55 These functional domains act as platforms for localizing and signaling of many membrane
56 proteins. Altering membrane cholesterol levels has been reported to affect the organization and
57 signaling of a number of receptors (Adkins *et al.* 2007; Arora *et al.* 2014; Bag *et al.* 2015; Brown
58 and London 1998; Pike 2003; Pucadyil and Chattopadhyay 2006). The actin cytoskeleton serves
59 as a structural element that can affect the functionality of membrane proteins, including their
60 oligomerization and transmembrane signaling (Kusumi *et al.* 2011).

61 Both cholesterol and the actin cytoskeleton have been reported to play a key role in
62 RAGE functions. For example Reddy *et al.* showed cholesterol depletion inhibited the S100-
63 induced effects involving RAGE in vascular smooth muscle cells and that intact caveolae are
64 necessary for RAGE signaling (Reddy *et al.* 2006). RAGE has also been reported to be part of
65 functional cholesterol-enriched domains in neural endothelial cells (Lisanti *et al.* 1994; Sbai *et*
66 *al.* 2010). Xiong *et al.* showed that the actin cytoskeleton played a pivotal role in RAGE-
67 mediated plasma membrane plasticity in a human umbilical vein endothelial cell line (Xiong *et*
68 *al.* 2011). They found that RAGE over expression reorganizes filamentous actin (F-actin) by
69 increasing β -catenin levels, resulting in inhibition of membrane sealing. Although it is evident
70 that cholesterol and the actin cytoskeleton affect some RAGE functions, possible roles in
71 affecting RAGE lateral diffusion remain unknown.

72 In this study, we have genetically fused monomeric red fluorescent protein (mRFP) to the
73 C-terminus of RAGE and measured its lateral diffusion using fluorescence recovery after
74 photobleaching (FRAP) in GM07373 endothelial cells. In FRAP, a small area on the cell
75 membrane is photobleached with a focused laser beam and the fluorescence recovery from the

76 diffusion of neighboring fluorescent molecules into the photobleached spot is recorded over
77 time. Several models have been constructed to extract diffusion parameters such as the immobile
78 population, diffusion coefficient and time-dependency of the diffusion (Feder *et al.* 1996; van
79 Zoelen *et al.* 1983). RAGE diffusion at native, cholesterol depleted and altered actin
80 cytoskeleton conditions have been studied. Methyl- β -cyclodextrin (M β CD) was used to deplete
81 cellular cholesterol. The actin cytoskeleton was altered using cytoskeletal drugs cytochalasin D
82 (CD) and Jasplakinolide (Jsp). Finally, signaling was measured by quantifying the
83 phosphorylation of extracellular-signal-regulated kinase (p-ERK) at native and altered cellular
84 conditions.

85

86 **MATERIALS & METHODS**

87 Cell culture

88 All experiments were performed using bovine artery GM07373 endothelial cells (Coriell
89 Institute Biorepositories, Camden, NJ). GM07373 cells were grown in complete growth medium
90 consisting of Dulbecco's modified Eagle's medium (DMEM) (Sigma-Aldrich, St. Louis, MO),
91 10% fetal bovine serum (FBS) (Irvine Scientific, Santa Ana, CA) and 12.5 mM Streptomycin
92 and 36.5 mM Penicillin (Fisher Scientific, Pittsburgh, PA) in a water-jacketed CO₂ incubator
93 (Thermo Scientific, Waltham, MA). Cells were sub-cultured using 0.25% (w/v) trypsin-EDTA
94 (Life Technology, Carlsbad, CA) solution every two days. All transfected GM07373 cells were
95 established to express respective recombinant proteins stably before any microscopy or
96 molecular biology experiments were performed. Plasmid and transfection details are in the
97 supplementary information.

98

99 Western blotting

100 GM07373 cells expressing RAGE (GM07373-RAGE) or RAGE-mRFP (GM07373-RAGE-
101 mRFP) were cultured to 100% confluence and rinsed with ice cold phosphate buffered saline
102 (PBS). Cells were lysed with RIPA buffer (150 mM sodium chloride, 1.0% NP-40 detergent,
103 0.5% sodium deoxycholate, 0.1% SDS, 50 mM Tris, pH 8.0) with Halt™ protease inhibitor
104 cocktail (1×, Thermo Scientific, Rockford, IL). After the initial lysis treatment, cells were passed
105 through a 21 gauge needle to ensure complete cell lysis. The protein mixture was first separated
106 on the NuPAGE® Novex® 4-12% Bis-Tris protein gel (Life Technology, Eugene, OR) and then
107 electro blotted onto Immun-Blot® LF PVDF membrane (Bio-Rad, Hercules, CA) as described
108 previously (Matsudaira 1989; Towbin *et al.* 1979). The PVDF membrane was probed following
109 the manufacturer's protocol (Bio-Rad). Antibodies used for probing were: anti-RAGE rabbit (H-
110 300, Santa Cruz Biotechnology), anti-RFP rabbit (Life Technology), anti-Vinculin goat (sc-7649,
111 Santa Cruz Biotechnology), anti-Actin rabbit (sc-1616-R, Santa Cruz Biotechnology), anti-p-
112 ERK rabbit (Tyr 204, sc-101761, Santa Cruz Biotechnology), anti-total-ERK 1/2 mouse (sc-
113 514302, Santa Cruz Biotechnology). The labeled secondary antibodies were Alexa Fluor 647
114 goat anti-rabbit (Life technologies), Alexa Fluor 488 donkey anti-goat (Life technologies), Alexa
115 Fluor 488 goat anti-mouse (Life technologies). Fluorescence was measured on a Typhoon FLA
116 9500 variable mode laser scanner (GE Healthcare, Waukesha, WI). The total-ERK and vinculin
117 protein bands were used as a loading control in Western blot experiments. The fluorescence
118 intensities were calculated from the 42 kDa band of p-ERK divided by the 42 kDa band of total-
119 ERK or the 42 kDa band of actin divided by the 130 kDa band of vinculin. The 42 kDa band of
120 ERK was used since it has a stronger intensity than the 44 kDa ERK band. All experiments were

121 performed in triplicate unless otherwise noted in figure legends. Reported p values were
122 calculated using the Student's t-test with a two-tailed homoscedastic distribution. Protein
123 sequences were analyzed by mass spectrometry as reported in the supplemental information.

124

125 FRAP sample preparation

126 Sterile glass bottom culture dishes were made by attaching a cover glass (22mm × 22mm, No.
127 1.5, Corning Inc., Corning, NY) to the bottom of a polystyrene petri dish (35mm × 10mm, Fisher
128 Scientific) containing a pre-drilled 3/4 inch diameter hole as described previously (Buster *et al.*
129 2010). GM07373-RAGE or GM07373-RAGE-mRFP cells were sub-cultured onto the culture
130 dishes two days before the experiment. Cells were either used without further treatment or
131 treated at 37 °C with MβCD (Sigma-Aldrich, 5mM, in serum free DMEM for 30 minutes) to
132 deplete the cholesterol or with CD (Sigma-Aldrich, 10 μM, in serum free DMEM for 60
133 minutes) or with Jsp (Santa Cruz Biotechnology, 3μM, in serum free DMEM for 30 minutes) to
134 alter the actin cytoskeleton as previously reported (Arora *et al.* 2014; Schwab *et al.* 2003; Shaw
135 and Tilney 1999) before the FRAP experiments.

136

137 FRAP Microscopy

138 All FRAP experiments were performed on a Nikon Eclipse TE2000U inverted microscope
139 (Nikon, Melville, NY) which was equipped with an oil-immersion objective (100×, Apo TIRF,
140 1.49 numerical aperture). The microscope was housed in a home built 0.9×0.6×0.5 m³ Plexiglas
141 box containing a heat source to maintain a 36 ± 2 °C at the sample throughout the experiment.
142 Fluorescence was excited with a mercury lamp (X-cite 120 PC, EXFO Photonic Solutions Inc.,
143 Mississauga, Ontario, Canada) operating at 25% of the power and an excitation filter

144 (HQ545/30x, Chroma Technology Corp., Bellows Falls, VT). The resulting fluorescence
145 emission was collected through an emission filter (HQ620/60x, Chroma Technology Corp.). For
146 photobleaching a region of the cell membrane, a 488-nm laser was directed to the sample with a
147 dichroic mirror (Q495lp, Chroma Technology Corp.). The laser power and photobleaching spot
148 diameter at the sample were 10 mW and 4.0 μm , respectively. A LabView program (National
149 Instruments, Austin, TX) was developed to control a shutter (Thorlabs, Jessup, MD) in the laser
150 path. The photobleaching time was 2 msec. Fluorescence images were recorded using a
151 PhotonMAX 512B EMCCD camera (Princeton Instruments, Trenton, NJ) and Winview
152 (Photometric, Tucson, AZ) image acquisition software. Ten pre-photobleach and 100 post-
153 photobleach images were collected with a time resolution of 410 ms per image. Dark-state
154 formation in mRFP is expected to have a negligible impact on the FRAP data collected on this
155 timescale. Data collection was completed within 1 h after adding imaging medium (pH=7.2, 155
156 mM NaCl, 5 mM KCl, 2 mM CaCl₂, 1 mM MgCl₂, 2 mM NaH₂PO₄, 10 mM HEPES and 10 mM
157 Glucose) to the cells.

158

159 FRAP data analysis

160 The fluorescence images collected pre-photobleach and post-photobleach were analyzed with
161 ImageJ (version 1.48, National Institute of Health) software. The fluorescence intensity from
162 three regions of interest (ROIs) was extracted for each image in the series of 110 images. The
163 ROIs were classified as the photobleached region (an area on the plasma membrane illuminated
164 by the laser spot), the non-photobleached region (an area on the plasma membrane away from
165 the photobleached region), and the background (an area where there was no cell present in the
166 field of view). Fluorescence recovery curves were constructed with a three-step process: (i) the

167 background intensity was subtracted from fluorescence intensities in the photobleached ROI, the
 168 resulting curves were normalized with the fluorescence intensities from (ii) the non-
 169 photobleached ROI and (iii) the average pre-photobleached intensity from the subsequently
 170 photobleached region to account for the lamp intensity fluctuations as well as photobleaching
 171 during the image acquisition period as described by Phair *et al.* (Phair *et al.* 2004). Fluorescence
 172 recovery curves were analyzed and the results were averaged over 24 to 53 cells for each data
 173 set. The number of cells measured was lower for Jsp, CD and MβCD data sets. These treatments
 174 result in a smaller average spread cell diameter, which reduces the number of cells that can be
 175 analyzed by FRAP compared to the untreated cells. Mobile fractions (*MF*) were calculated using
 176 equation 1.

$$MF = \frac{F_{\infty} - F_0}{F^0 - F_0} \times 100 \quad (1)$$

178 Where F_0 is the intensity immediately after photobleaching, F^0 is the pre-photobleaching
 179 intensity and F_{∞} is the final intensity (i.e., in image 110), where all fluorescence intensities refer
 180 to the values from the fluorescence recovery curves. Each fluorescence recovery curve was
 181 further fit to equation 2 using IGOR Pro V 6.32A (WaveMetrics Inc., Lake Oswego, OR) to
 182 measure the time dependency of the fluorescence recovery as well as diffusion coefficients
 183 (Feder *et al.* 1996).

$$F(t) = \frac{F_0 + F_{\infty} \left(\frac{t}{\tau}\right)^{\alpha}}{1 + \left(\frac{t}{\tau}\right)^{\alpha}} \quad (2)$$

186 Where $F(t)$ is the fluorescence intensity at time t , α is the time exponent and τ is time for 50%
 187 fluorescence recovery. Diffusion coefficients were calculated using equation 3.

$$D(t) = \frac{\omega^2}{4\tau^{\alpha} t^{(\alpha-1)}} \quad (3)$$

190 Where $D(t)$ is the diffusion coefficient at time t and ω is the radius of the photobleached spot.
191 The statistical significance of all reported data sets was calculated using first the F-test at the
192 95% confidence level and then the homoscedastic/heteroscedastic (as determined from the F-
193 test) Student's t-test with a two-tailed distribution. The resulting p values that indicate statistical
194 differences are reported in Figure 7; statistical differences at the 95% confidence level (i.e., p
195 values below 0.05) are considered significant. Diffusion parameters are presented as box-and-
196 whisker plots. For box-and-whisker plots, the boundary of the box shows the twenty-fifth and
197 seventy-fifth quartiles. A line and a triangle within the box indicate the median and the mean,
198 respectively. Whiskers above and below the boxes are 1.5 times the interquartile range.

199

200 Actin cytoskeleton staining

201 Cells were sub-cultured onto glass-bottom petri dishes and allowed to spread in the incubator for
202 two days before the experiment. Cells were treated as described above with 5 mM M β CD, 10
203 μ M CD, or 3 μ M Jsp before the actin cytoskeleton was stained for fluorescence imaging. The
204 staining protocol was described previously (Syed *et al.* 2014). Briefly, cells were fixed with 4%
205 (w/v) paraformaldehyde in PBS for 10 minutes. Triton X-100 (0.1% (v/v) in PBS) was used for
206 cell membrane permeabilization. Blocking was performed using bovine serum albumin (1% (w/v)
207 in PBS) for 5 minutes. Cells were further incubated with Atto 647N conjugated phalloidin
208 (Sigma-Aldrich) to stain the F-actin overnight at 4 °C. Stained cells were rinsed with imaging
209 medium before imaging using the Nikon Eclipse TE2000U inverted microscope described above.
210 The actin cytoskeleton was further quantified to measure the alignment in the actin fibers in 21 to
211 41 cells. Alignment was calculated using an ImageJ plugin, FibrilTool, as described previously
212 (Boudaoud *et al.* 2014).

213

214

215 **Results and Discussion**

216 *Characterization of RAGE and RAGE-mRFP Expression*

217 The primary goal of this study is to probe the lateral diffusion of RAGE in the GM07373 cell
218 membrane in order to characterize the role of the actin cytoskeletal and cholesterol in altering
219 RAGE diffusion. To achieve this goal, plasmids were transfected into GM07373 cells to stably
220 express full-length RAGE or RAGE-mRFP. RAGE or RAGE-mRFP expression was confirmed
221 by Western blot analysis of cell lysates as shown in Fig. 1. A protein band corresponding to
222 RAGE at ~55 kDa (band 1, Fig. 1) was observed in the GM07373-RAGE cell lysate (lane b, Fig.
223 1) but not in the GM07373 cell lysate (lane a, Fig. 1). Surprisingly, the GM07373-RAGE-mRFP
224 cell lysate (lane c, Fig. 1) showed three bands in the 60 to 80 kDa molecular weight range after
225 probing the membrane with the RAGE primary antibody. Bands 1 to 4 were positive for RAGE
226 peptides as measured by mass spectrometry. After the PVDF membrane was probed with a
227 polyclonal mRFP antibody, only a single band was observed from the GM07373-RAGE-mRFP
228 cell lysate (band 5, Fig. 1) near the molecular weight of band 3. It was confirmed by fluorescence
229 imaging of the PVDF membrane that fluorescence was measured only at the location of band 5,
230 thus RAGE-containing bands 2 and 4 do not contribute to the fluorescence microscopy results
231 reported below.

232 Phosphorylation of extracellular-signal-regulated kinase (p-ERK) was used as a marker
233 for downstream RAGE signaling (Huttunen *et al.* 2002; Zong *et al.* 2010). There was no
234 statistically significant difference in p-ERK levels in cells expressing RAGE or RAGE-mRFP

235 (Fig. 2), indicating that the mRFP tag on RAGE did not alter p-ERK signaling in GM07373
236 cells.

237

238 *RAGE-mRFP diffusion in the native GM07373 cell membrane*

239 FRAP experiments on GM07373 cells expressing RAGE-mRFP were performed and the average
240 recovery curve from 24-53 cells is shown in Online Resource 1 (Fig. S1). Each replicate curve
241 was individually fit to the time-dependent diffusion model with an immobile fraction (i.e., all
242 parameters α , F_0 , F_∞ and τ in equation 2 were allowed to vary) as described by Federer *et al.*
243 (Feder *et al.* 1996). The time exponent (α) from the fit parameters provides information on the
244 nature of the mode of diffusion. An α value of 1 indicates time-independent Brownian diffusion,
245 whereas a value less than 1 indicates time-dependent diffusion. The average α value measured
246 for RAGE-mRFP was 0.9 (Fig. 7). The average mobile fraction was 90% and the average
247 diffusion coefficient was $0.3 \mu\text{m}^2/\text{s}$ for RAGE-mRFP at native cellular conditions. While FRAP
248 provides a measure of the average diffusion properties of RAGE-mRFP, it is known that RAGE
249 diffusion is heterogeneous (Syed *et al.* 2016). For example, when the diffusion coefficient is
250 measured one receptor at a time across 100 receptors, the diffusion coefficient varies by over 4
251 orders of magnitude. The heterogeneity in RAGE diffusion is not detectable with the ensemble
252 FRAP method. On the other hand, FRAP measurements yield the fraction of mobile RAGE,
253 which has not been possible to measure with other analysis techniques (Syed *et al.* 2016).

254

255 *Alterations to the F-actin cytoskeleton alter RAGE-mRFP diffusion properties measured by*
256 *FRAP*

257 To study the possible effect of the actin cytoskeleton on RAGE lateral diffusion, the actin
258 cytoskeleton was altered with two drugs, CD and Jsp. CD depolymerizes the filamentous actin
259 cytoskeleton and prevents repolymerization by binding to actin monomers (Casella *et al.* 1981).
260 Jsp binds with filamentous actin and inhibits depolymerization (Spector *et al.* 1999). Atto 647N
261 conjugated phalloidin was used to measure the effect of CD and Jsp on the actin cytoskeleton in
262 GM07373-RAGE cells as shown in Fig. 3. In the native GM07373 cells, the actin cytoskeleton
263 staining generated partially aligned fibers with a well-defined cell boundary as shown in Fig. 3a.
264 After the CD treatment, the actin structure was significantly altered and no clear cell boundary
265 was observed (Fig. 3c). Jsp binds to the actin cytoskeleton in competition with the Atto 647N
266 conjugated phalloidin (Bubb *et al.* 2000). Hence, Atto 647N phalloidin actin cytoskeleton
267 staining was diminished for Jsp treated cells (Fig. 3d). There was no change in the actin
268 expression as measured from Western blot analysis of the cell lysate treated with CD or Jsp (Fig.
269 4).

270 RAGE-mRFP diffusion parameters were measured for CD or Jsp treated cells. The
271 RAGE-mRFP mobile fraction and diffusion coefficient were decreased by 22% and 37%,
272 respectively, when the actin cytoskeleton was altered with Jsp (Fig. 7). In contrast, CD treatment
273 does not alter the RAGE diffusion properties. Jsp and CD have opposite effects on the
274 polymerization of the actin cytoskeleton. Jsp hinders depolymerization, whereas CD
275 depolymerizes the actin filaments. Jsp results in less mobile and slower RAGE, suggesting an
276 actin cytoskeleton fixed in a polymerized state slows RAGE diffusion and reduces the mobile
277 fraction. Surprisingly, CD treatment to depolymerize the actin cytoskeleton does not statistically
278 increase RAGE mobility as measured by FRAP; although it is noteworthy that prior to altering

279 the actin cytoskeleton RAGE diffusion is already relatively unhindered with a large mobile
280 fraction and nearly Brownian behavior as indicated by the α value.

281 To understand if RAGE diffusion properties are linked to downstream signaling,
282 phosphorylation of ERK (p-ERK) was measured in both GM07373 and GM07373-RAGE cells
283 after CD and Jsp treatment. p-ERK was decreased by 70% and 50% in GM07373-RAGE cells
284 when the actin cytoskeleton was disrupted with CD and JSP, respectively (Fig. 5a and b). There
285 was no statistically significant change in p-ERK observed in GM07373 cells lacking detectable
286 RAGE expression after CD or Jsp treatment (Fig. 5c and d). This indicates that the downstream
287 signaling of RAGE is altered when the actin cytoskeleton is disrupted, regardless of the effects
288 disrupting the actin cytoskeleton has on RAGE diffusion.

289 To investigate the effect of cholesterol on the lateral diffusion of RAGE-mRFP,
290 cholesterol was depleted using M β CD. The total free cholesterol was depleted by 45% and no
291 statistically significant change in the endogenous cholesterol ester was observed when cells were
292 incubated with 5 mM M β CD as measured by Amplex[®] Red cholesterol quantification assay
293 (Fig. 6a). The diffusion parameters statistically unchanged for RAGE-mRFP (Fig. 7). There was
294 also no change in p-ERK measured after cholesterol depletion from both GM07373-RAGE cells
295 and GM07373 (Fig. 6b-d). These conclusions are valid in the absence of RAGE ligand. In the
296 presence of ligand, RAGE signaling may be dependent on cholesterol as previously reported
297 (Reddy *et al.* 2006).

298 It has been previously reported that a change in membrane cholesterol not only affects the
299 cell membrane structure but also has a global effect, including reorganization of the actin
300 structure (Kwik *et al.* 2003). This appears to be valid in GM07373-RAGE cells (Fig. 3 a and b).

301 A significant 40% decrease in the actin fiber alignment was measured after cholesterol depletion
302 in both the GM07373-RAGE and GM07373 cell lines. No change in the actin expression was
303 observed with cholesterol depletion (Fig. 6). These observations indicate that cholesterol
304 depletion affects the actin cytoskeleton organization, but the cholesterol-depletion-induced
305 changes to the actin cytoskeleton alignment are not associated with changes in RAGE diffusion
306 properties.

307 In summary, RAGE-mRFP diffuses in the cell membrane with a large mobile fraction at
308 native GM07373 cellular conditions. The depolymerization of the actin cytoskeleton plays a role
309 in how RAGE diffuses in the membrane, and more generally, the actin cytoskeleton
310 polymerization dynamics alter the downstream signaling of RAGE. Even though there is a
311 significant change in the actin cytoskeleton alignment as revealed by phalloidin staining,
312 cholesterol depletion has no effect on RAGE lateral diffusion as measured by FRAP or signaling
313 as measured by p-ERK. The combined data point to an important role for actin depolymerization
314 in the diffusion properties of RAGE and a link between the actin cytoskeleton and RAGE-
315 mediated p-ERK signaling.

316

317 **Acknowledgements**

318 This work was supported by the National Science Foundation (CHE- 1412084). The authors
319 thank Joel Nott of the protein facility at Iowa State University for help with mass spectrometry,
320 and Dipak Mainali and Chamari Wijesoorya for their assistance with cell culture.

321

322 **References**

- 323 Adkins EM, Samuvel DJ, Fog JU, Eriksen J, Jayanthi LD, Vaegter CB, Ramamoorthy S, Gether
324 U (2007) Membrane mobility and microdomain association of the dopamine transporter
325 studied with fluorescence correlation spectroscopy and fluorescence recovery after
326 photobleaching. *Biochemistry* 46:10484-10497
- 327 Ando J, Kinoshita M, Cui J, Yamakoshi H, Dodo K, Fujita K, Murata M, Sodeoka M (2015)
328 Sphingomyelin distribution in lipid rafts of artificial monolayer membranes visualized by
329 Raman microscopy. *Proc Natl Acad Sci U S A* 112:4558-4563
- 330 Arora N, Syed A, Sander S, Smith EA (2014) Single particle tracking with sterol modulation
331 reveals the cholesterol-mediated diffusion properties of integrin receptors. *Phys Biol*
332 11:066001
- 333 Axelrod D (1983) Lateral motion of membrane proteins and biological function. *Journal of*
334 *Membrane Biology* 75:10
- 335 Bag N, Huang S, Wohland T (2015) Plasma Membrane Organization of Epidermal Growth
336 Factor Receptor in Resting and Ligand-Bound States. *Biophys J* 109:1925-1936
- 337 Barile GR, Schmidt AM (2007) RAGE and its ligands in retinal disease. *Curr Mol Med* 7:758-
338 765
- 339 Basta G (2008) Receptor for advanced glycation endproducts and atherosclerosis: From basic
340 mechanisms to clinical implications. *Atherosclerosis* 196:9-21
- 341 Bierhaus A, Nawroth PP (2009) Multiple levels of regulation determine the role of the receptor
342 for AGE (RAGE) as common soil in inflammation, immune responses and diabetes
343 mellitus and its complications. *Diabetologia* 52:2251-2263
- 344 Boudaoud A, Burian A, Borowska-Wykret D, Uyttewaal M, Wrzalik R, Kwiatkowska D,
345 Hamant O (2014) FibrilTool, an ImageJ plug-in to quantify fibrillar structures in raw
346 microscopy images. *Nat Protoc* 9:457-463
- 347 Briot R, Frank JA, Uchida T, Lee JW, Calfee CS, Matthay MA (2009) Elevated levels of the
348 receptor for advanced glycation end products, a marker of alveolar epithelial type I cell
349 injury, predict impaired alveolar fluid clearance in isolated perfused human lungs. *Chest*
350 135:269-275
- 351 Brown DA, London E (1998) Functions of lipid rafts in biological membranes. *Annu Rev Cell*
352 *Dev Biol* 14:111-136
- 353 Bubb MR, Spector I, Beyer BB, Fosen KM (2000) Effects of jasplakinolide on the kinetics of
354 actin polymerization. An explanation for certain in vivo observations. *J Biol Chem*
355 275:5163-5170
- 356 Buster DW, Nye J, Klebba JE, Rogers GC (2010) Preparation of Drosophila S2 cells for light
357 microscopy. *J Vis Exp*
- 358 Casella JF, Flanagan MD, Lin S (1981) Cytochalasin D inhibits actin polymerization and induces
359 depolymerization of actin filaments formed during platelet shape change. *Nature*
360 293:302-305
- 361 Feder TJ, Brust-Mascher I, Slattery JP, Baird B, Webb WW (1996) Constrained diffusion or
362 immobile fraction on cell surfaces: a new interpretation. *Biophys J* 70:2767-2773
- 363 Ganguly S, Pucadyil TJ, Chattopadhyay A (2008) Actin cytoskeleton-dependent dynamics of the
364 human serotonin1A receptor correlates with receptor signaling. *Biophys J* 95:451-463

365 Ghavami S, Rashedi I, Dattilo BM, Eshraghi M, Chazin WJ, Hashemi M, Wesselborg S,
366 Kerkhoff C, Los M (2008) S100A8/A9 at low concentration promotes tumor cell growth
367 via RAGE ligation and MAP kinase-dependent pathway. *J Leukoc Biol* 83:1484-1492
368 Hermani A, De Servi B, Medunjanin S, Tessier PA, Mayer D (2006) S100A8 and S100A9
369 activate MAP kinase and NF-kappaB signaling pathways and trigger translocation of
370 RAGE in human prostate cancer cells. *Exp Cell Res* 312:184-197
371 Hofmann MA, Drury S, Fu C, Qu W, Taguchi A, Lu Y, Avila C, Kambham N, Bierhaus A,
372 Nawroth P, Neurath MF, Slattery T, Beach D, McClary J, Nagashima M, Morser J, Stern
373 D, Schmidt AM (1999) RAGE mediates a novel proinflammatory axis: a central cell
374 surface receptor for S100/calgranulin polypeptides. *Cell* 97:889-901
375 Huttunen HJ, Fages C, Rauvala H (1999) Receptor for advanced glycation end products
376 (RAGE)-mediated neurite outgrowth and activation of NF-kappaB require the
377 cytoplasmic domain of the receptor but different downstream signaling pathways. *J Biol*
378 *Chem* 274:19919-19924
379 Huttunen HJ, Kuja-Panula J, Rauvala H (2002) Receptor for advanced glycation end products
380 (RAGE) signaling induces CREB-dependent chromogranin expression during neuronal
381 differentiation. *J Biol Chem* 277:38635-38646
382 Koch M, Chitayat S, Dattilo BM, Schiefner A, Diez J, Chazin WJ, Fritz G (2010) Structural
383 basis for ligand recognition and activation of RAGE. *Structure* 18:1342-1352
384 Kusumi A, Suzuki KG, Kasai RS, Ritchie K, Fujiwara TK (2011) Hierarchical mesoscale
385 domain organization of the plasma membrane. *Trends Biochem Sci* 36:604-615
386 Kwik J, Boyle S, Fooksman D, Margolis L, Sheetz MP, Edidin M (2003) Membrane cholesterol,
387 lateral mobility, and the phosphatidylinositol 4,5-bisphosphate-dependent organization of
388 cell actin. *Proceedings of the National Academy of Sciences* 100:13964-13969
389 Lander HM, Tauras JM, Ogiste JS, Hori O, Moss RA, Schmidt AM (1997) Activation of the
390 receptor for advanced glycation end products triggers a p21(ras)-dependent mitogen-
391 activated protein kinase pathway regulated by oxidant stress. *J Biol Chem* 272:17810-
392 17814
393 Leclerc E, Fritz G, Vetter SW, Heizmann CW (2009) Binding of S100 proteins to RAGE: an
394 update. *Biochim Biophys Acta* 1793:993-1007
395 Lingwood D, Simons K (2010) Lipid rafts as a membrane-organizing principle. *Science* 327:46-
396 50
397 Lisanti MP, Scherer PE, Vidugiriene J, Tang Z, Hermanowski-Vosatka A, Tu YH, Cook RF,
398 Sargiacomo M (1994) Characterization of caveolin-rich membrane domains isolated from
399 an endothelial-rich source: implications for human disease. *J Cell Biol* 126:111-126
400 Logsdon CD, Fuentes MK, Huang EH, Arumugam T (2007) RAGE and RAGE ligands in
401 cancer. *Curr Mol Med* 7:777-789
402 Matsudaira PT (1989) Strategies for obtaining partial amino acid sequence data. In a practical
403 guide to protein and peptide purification for microsequencing. Academic Press, New
404 York, pp 29-30
405 Phair RD, Gorski SA, Misteli T (2004) Measurement of dynamic protein binding to chromatin in
406 vivo, using photobleaching microscopy. *Methods Enzymol* 375:393-414
407 Pike LJ (2003) Lipid rafts: bringing order to chaos. *J Lipid Res* 44:655-667
408 Pucadyil TJ, Chattopadhyay A (2006) Role of cholesterol in the function and organization of G-
409 protein coupled receptors. *Prog Lipid Res* 45:295-333

410 Reddy MA, Li SL, Sahar S, Kim YS, Xu ZG, Lanting L, Natarajan R (2006) Key role of Src
411 kinase in S100B-induced activation of the receptor for advanced glycation end products
412 in vascular smooth muscle cells. *J Biol Chem* 281:13685-13693

413 Ronchi P, Colombo S, Francolini M, Borgese N (2008) Transmembrane domain-dependent
414 partitioning of membrane proteins within the endoplasmic reticulum. *J Cell Biol* 181:105-
415 118

416 Sbai O, Devi TS, Melone MA, Feron F, Khrestchatsky M, Singh LP, Perrone L (2010) RAGE-
417 TXNIP axis is required for S100B-promoted Schwann cell migration, fibronectin
418 expression and cytokine secretion. *J Cell Sci* 123:4332-4339

419 Schmidt AM, Vianna M, Gerlach M, Brett J, Ryan J, Kao J, Esposito C, Hegarty H, Hurley W,
420 Clauss M, *et al.* (1992) Isolation and characterization of two binding proteins for
421 advanced glycosylation end products from bovine lung which are present on the
422 endothelial cell surface. *J Biol Chem* 267:14987-14997

423 Schwab UE, Ribeiro CM, Neubauer H, Boucher RC (2003) Role of actin filament network in
424 *Burkholderia multivorans* invasion in well-differentiated human airway epithelia. *Infect*
425 *Immun* 71:6607-6609

426 Shaw MK, Tilney LG (1999) Induction of an acrosomal process in *Toxoplasma gondii*:
427 visualization of actin filaments in a protozoan parasite. *Proc Natl Acad Sci U S A*
428 96:9095-9099

429 Simons K, Gerl MJ (2010) Revitalizing membrane rafts: new tools and insights. *Nat Rev Mol*
430 *Cell Biol* 11:688-699

431 Spector I, Braet F, Shochet NR, Bubb MR (1999) New anti-actin drugs in the study of the
432 organization and function of the actin cytoskeleton. *Microsc Res Tech* 47:18-37

433 Syed A, Lesoine MD, Bhattacharjee U, Petrich JW, Smith EA (2014) The number of
434 accumulated photons and the quality of stimulated emission depletion lifetime images.
435 *Photochem Photobiol* 90:767-772

436 Syed A, Zhu Q, Smith EA (2016) Ligand binding affinity and changes in the lateral diffusion of
437 receptor for advanced glycation endproducts (RAGE). *Biochim Biophys Acta* 1858:3141-
438 3149

439 Taguchi A, Blood DC, del Toro G, Canet A, Lee DC, Qu W, Tanji N, Lu Y, Lalla E, Fu C,
440 Hofmann MA, Kislinger T, Ingram M, Lu A, Tanaka H, Hori O, Ogawa S, Stern DM,
441 Schmidt AM (2000) Blockade of RAGE-amphoterin signalling suppresses tumour
442 growth and metastases. *Nature* 405:354-360

443 Towbin H, Staehelin T, Gordon J (1979) Electrophoretic transfer of proteins from
444 polyacrylamide gels to nitrocellulose sheets: procedure and some applications. *Proc Natl*
445 *Acad Sci U S A* 76:4350-4354

446 van Zoelen EJ, Tertoolen LG, de Laat SW (1983) Simple computer method for evaluation of
447 lateral diffusion coefficients from fluorescence photobleaching recovery kinetics.
448 *Biophys J* 42:103-108

449 Veya L, Piguat J, Vogel H (2015) Single Molecule Imaging Deciphers the Relation between
450 Mobility and Signaling of a Prototypical G Protein-coupled Receptor in Living Cells.
451 *Journal of Biological Chemistry* 290:27723-27735

452 Wang L, Li S, Jungalwala FB (2008) Receptor for advanced glycation end products (RAGE)
453 mediates neuronal differentiation and neurite outgrowth. *J Neurosci Res* 86:1254-1266

454 Xiong F, Leonov S, Howard AC, Xiong S, Zhang B, Mei L, McNeil P, Simon S, Xiong WC
455 (2011) Receptor for advanced glycation end products (RAGE) prevents endothelial cell

456 membrane resealing and regulates F-actin remodeling in a beta-catenin-dependent
457 manner. *J Biol Chem* 286:35061-35070

458 Yan SD, Bierhaus A, Nawroth PP, Stern DM (2009) RAGE and Alzheimer's disease: a
459 progression factor for amyloid-beta-induced cellular perturbation? *J Alzheimers Dis*
460 16:833-843

461 Yan SD, Chen X, Fu J, Chen M, Zhu H, Roher A, Slattery T, Zhao L, Nagashima M, Morser J,
462 Migheli A, Nawroth P, Stern D, Schmidt AM (1996) RAGE and amyloid-beta peptide
463 neurotoxicity in Alzheimer's disease. *Nature* 382:685-691

464 Yeh CH, Sturgis L, Haidacher J, Zhang XN, Sherwood SJ, Bjorcke RJ, Juhasz O, Crow MT,
465 Tilton RG, Denner L (2001) Requirement for p38 and p44/p42 mitogen-activated protein
466 kinases in RAGE-mediated nuclear factor-kappaB transcriptional activation and cytokine
467 secretion. *Diabetes* 50:1495-1504

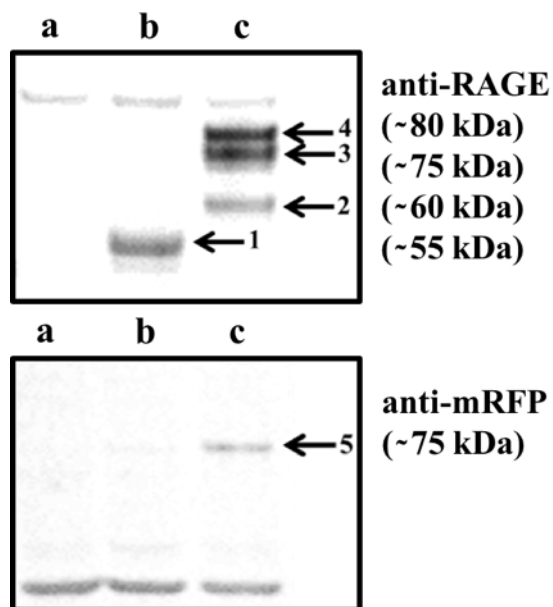
468 Zong H, Madden A, Ward M, Mooney MH, Elliott CT, Stitt AW (2010) Homodimerization is
469 essential for the receptor for advanced glycation end products (RAGE)-mediated signal
470 transduction. *J Biol Chem* 285:23137-23146

471

472

473

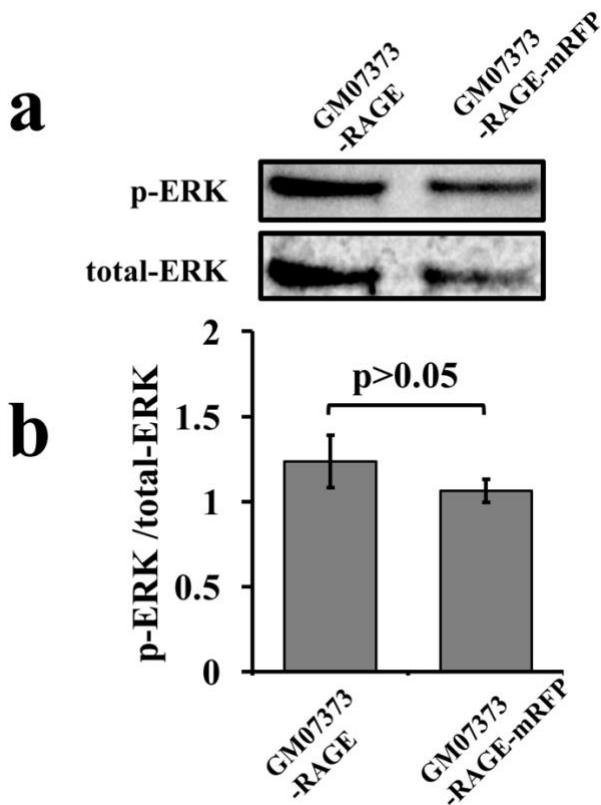
474 **Figures**



475

476 Figure 1. Western blot analysis of (a) GM07373 cell lysate, (b) GM07373-RAGE cell lysate, and
477 (c) GM07373-RAGE-mRFP cell lysate. (Top) fluorescence image of the PVDF membrane
478 probed with anti-RAGE antibody; (bottom) fluorescence image of the PVDF membrane probed
479 with anti-mRFP antibody. Unlabeled bands (three upper bands in the top image and three lower
480 bands in the bottom image) are present in all lanes and likely represent non-specific interactions
481 of antibodies.

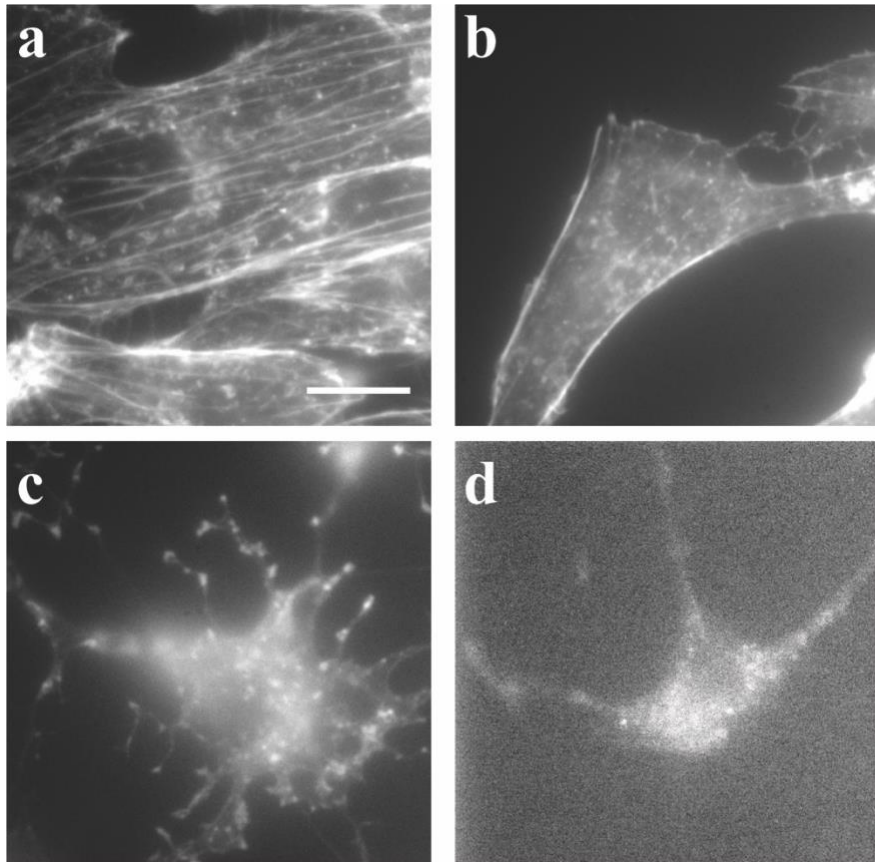
482



483

484 Figure 2. Western blot analysis of phosphorylation of ERK and total-ERK expression in the
 485 GM07373-RAGE cell lysate and GM07373-RAGE-mRFP cell lysate. (a) Fluorescence image of
 486 the PVDF membrane probed with anti-p-ERK or anti-total-ERK antibody. (b) Average (n = 3)
 487 fluorescence intensities of the 42 kDa band of p-ERK divided by the 42 kDa total-ERK band.
 488 Error bars represent one standard deviation.

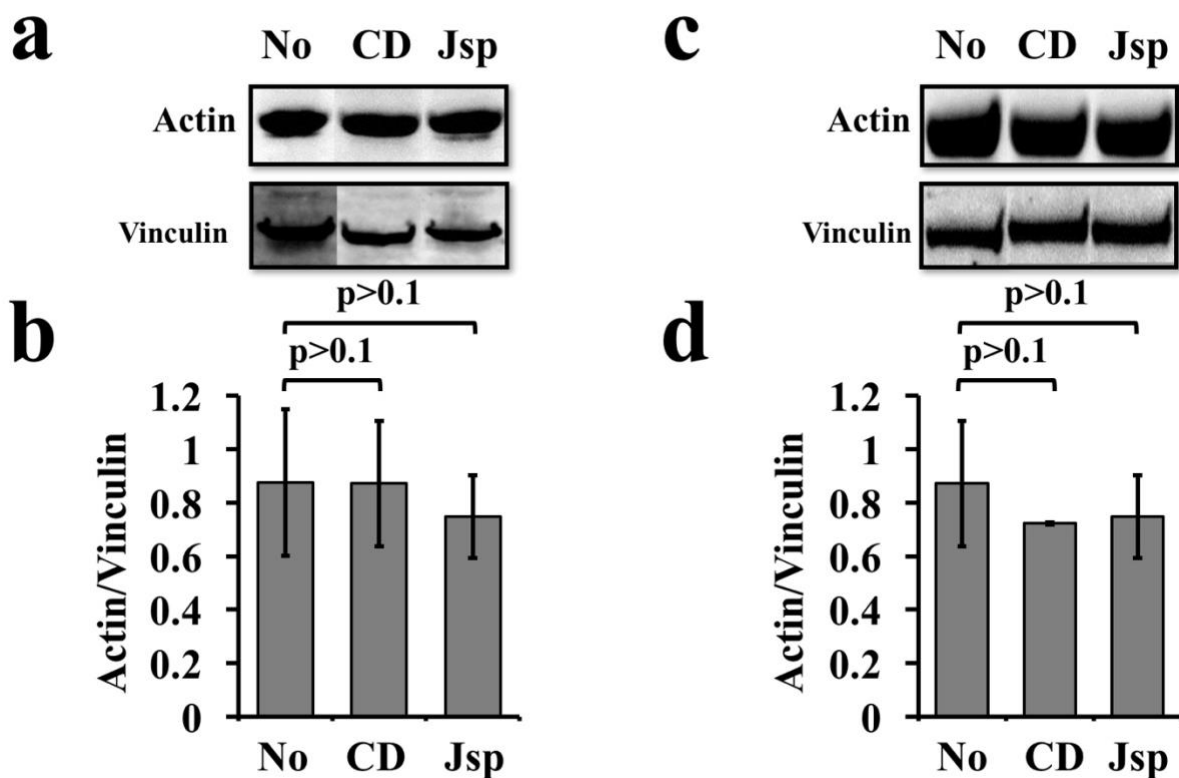
489



490

491 Figure 3. Fluorescence images of GM07373-RAGE cells with the actin cytoskeleton stained with
492 Atto 647N conjugated phalloidin. (a) No treatment, (b) 5 mM methyl- β -cyclodextrin treatment,
493 (c) 10 μ M cytochalasin-D treatment, or (d) 3 μ M Jasplakinolide treatment. The intensity scales
494 are: (a) and (b) 1700 to 7000 intensity units, (c) 1500 to 3000 intensity units, and (d) 1500 to
495 1700 intensity units. The scale bar is 20 μ m and is the same for all images.

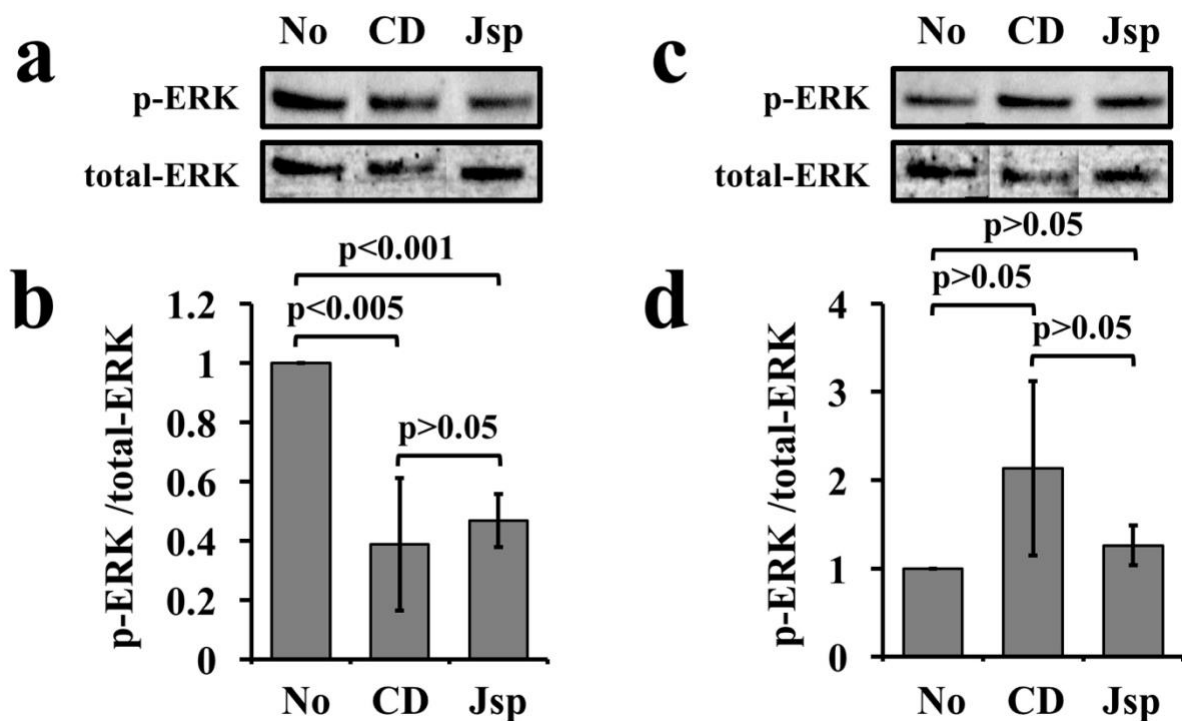
496



497

498 Figure 4. Western blot analysis of actin expression in the (a, b) GM07373-RAGE and (c, d)
 499 GM07373 cell lysate with no treatment (No), 10 μ M cytochalasin D (CD) treatment, or 3 μ M
 500 Jasplakinolide (Jsp) treatment. (a, c) Fluorescence image of the PVDF membrane probed with
 501 anti-actin or anti-vinculin antibody. (b, d) Average ($n = 3$) fluorescence intensities of the actin
 502 band divided by the vinculin band. Error bars represent one standard deviation.

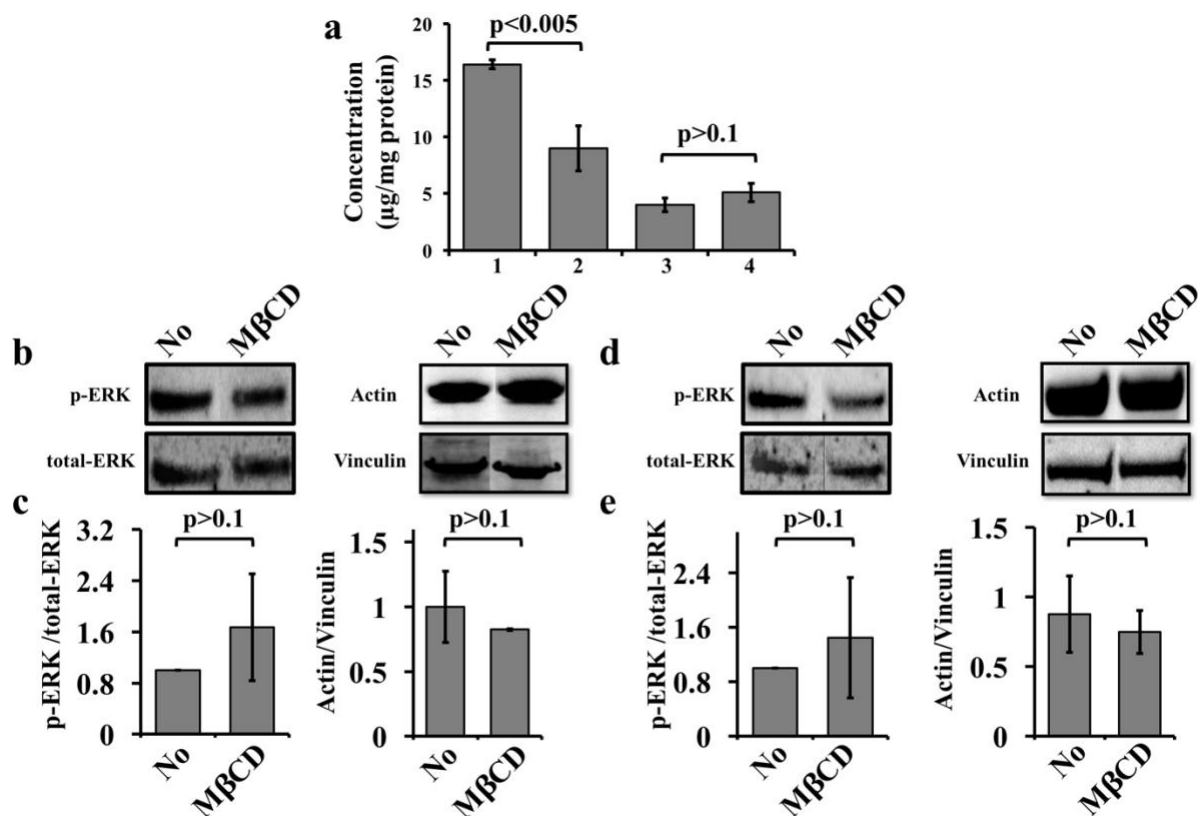
503



504

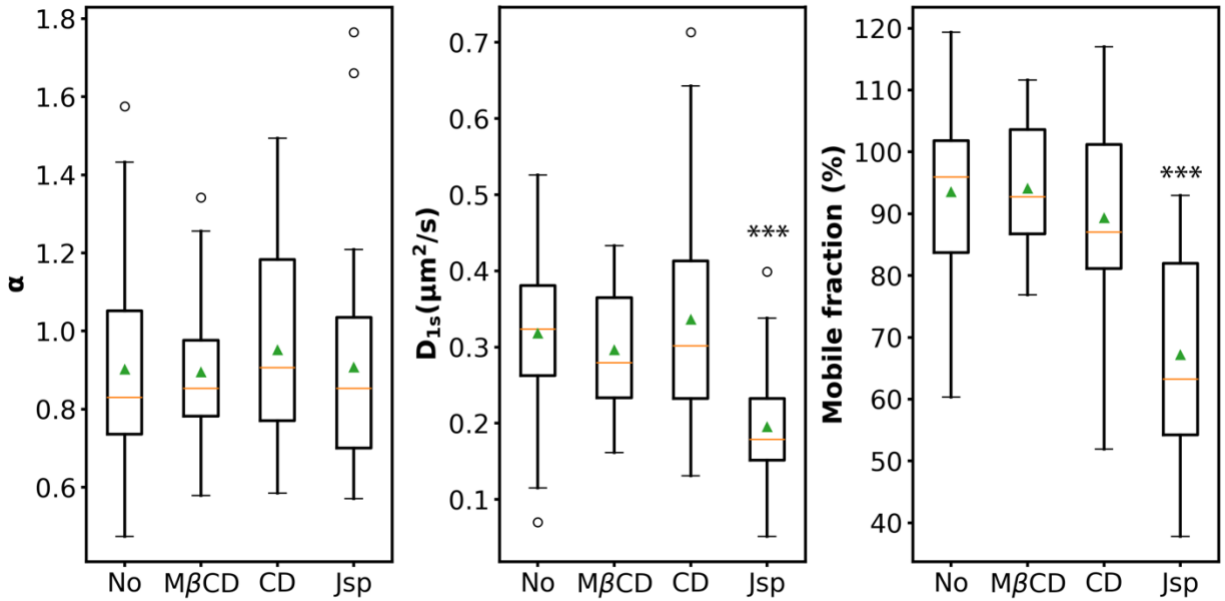
505 Figure 5. Western blot analysis of phosphorylation of ERK and total-ERK expression in the (a,
 506 b) GM07373-RAGE and (c, d) GM07373 cell lysate with no treatment (No), 10 μ M cytochalasin
 507 D (CD) treatment, or 3 μ M Jasplakinolide (Jsp) treatment. (a, c) Fluorescence image of the
 508 PVDF membrane probed with anti-p-ERK or anti-total-ERK antibody. (b, d) Average ($n = 3$)
 509 fluorescence intensities of the 42 kDa band of p-ERK divided by the 42 kDa total-ERK band.
 510 The band intensities were normalized to the no treatment band. Error bars represent one standard
 511 deviation.

512



513
 514 Figure 6. (a) Cholesterol quantification with Amplex® Red assay. Average (n = 2) free
 515 cholesterol (1 and 2) and cholesterol ester (3 and 4) concentration as measured from GM07373-
 516 RAGE cell lysate at native cellular conditions (1 and 3) and 5 mM methyl-β-cyclodextrin
 517 (MβCD) treated (2 and 4). Effect of MβCD treatment on (b, c) GM07373-RAGE cells and (d, e)
 518 GM07373 cells. (b, d) Fluorescence image of the PVDF membrane probed with anti-p-ERK,
 519 anti-total-ERK, anti-actin or anti-vinculin antibody. (c, e) Average (n=4) fluorescence intensities
 520 of the 42 kDa band of p-ERK divided by the 42 kDa total-ERK band (left); Average (n=2)
 521 fluorescence intensities of the actin band divided by the vinculin band (right). Error bars
 522 represent one standard deviation.

523



524

525

526 Figure 7. Box-and-whisker plots ($n = 24$ to 53) of RAGE-mRFP diffusion parameters in the
 527 GM07373 cell membrane obtained by FRAP after no treatment (No), 5 mM methyl- β -
 528 cyclodextrin (M β CD) treatment, 10 μM cytochalasin D (CD) treatment, or 3 μM Jasplakinolide
 529 (Jsp) treatment. The median and mean are represented as a horizontal line and triangle,
 530 respectively. The box limits are 50% (25–75%), the whiskers indicates 1.5 times the interquartile
 531 range, and the outliers are shown as open circles. *** indicates a statistically different from no
 532 treatment at the $p < 0.001$ level.

533